Journal of Natural Gas Science and Engineering 76 (2020) 103223

Contents lists available at ScienceDirect

Journal of Natural Gas Science and Engineering

journal homepage: http://www.elsevier.com/locate/jngse

Upwarding gas source and postgenetic processes in the shallow sediments from the ARAON Mounds, Chukchi Sea

Ji-Hoon Kim [a,*,1], Akihiro Hachikubo [b,1], Masato Kida [b], Hirotsugu Minami [b], Dong-Hun Lee [c], Young Keun Jin [d], Jong-Sik Ryu [e], Yung Mi Lee [d], Jin Hur [f], Myong-Ho Park [g], Young-Gyun Kim [h], Moo-Hee Kang [a], Sanghee Park [i], Meilian Chen [j], Seung-Goo Kang [d], Sookwan Kim [d]

[a] Petroleum and Marine Resources Research Division, Korea Institute of Geoscience and Mineral Resources, 124 Gwahang-no Yuseong-gu, Daejeon 34312, South Korea
[b] Environmental and Energy Resources Research Center, Kitami Institute of Technology, 165 Koen-cho, Kitami 090-8507, Japan
[c] Department of Marine Sciences and Convergent Technology, Hanyang University ERICA Campus 15588, South Korea
[d] Korea Polar Research Institute, 26 Songdomirae-ro, Yeonsu-gu, Incheon 21990, South Korea
[e] Department of Earth and Environmental Sciences, Pukyong National University, Busan 48513, South Korea
[f] Department of Environment & Energy, Sejong University, Seoul 05006, South Korea
[g] Department of Earth System Sciences, Yonsei University, Seoul 03722, South Korea
[h] Research Institute for Earth Resources, Kangwon National University, Gangwon-do 24341, South Korea
[i] Division of Earth and Environment Sciences, Korea Basic Science Institute, Chungbuk 28119, South Korea
[j] Environmental Program, Guangdong Technion - Israel Institute of Technology, Shantou 515063, China

ARTICLE INFO

Keywords:
Arctic Ocean
ARAON Mounds
Thermogenic gas
Upward gas migration
Carbon isotopic fractionation

ABSTRACT

The methane (CH_4) emission from the Arctic Ocean is crucial to understand global carbon cycle. Here, we investigated sulfate (SO_4^{2-}) in pore water and compositional and isotopic gas signatures at ARAON Mounds (hydrate/nonhydrate-bearing sites) and background site in the Chukchi Sea. Sulfate-methane transition (SMT) did not reach at the background site but occurred at shallow depths (≤3.3 m below the seafloor) at all ARAON Mounds sites. The SO_4^{2-} profiles at ARAON Mounds also clearly indicate the unsteady state due to upward gas migration by high flux at the hydrate-bearing sites compared to the nonhydrate-bearing sites. The isotopic signatures of gas samples at the hydrate-bearing sites and below the SMT at the nonhydrate-bearing sites reflect thermogenic source transported across at least 1 km through faults/fractures in the Chukchi Sea. The headspace (HS) gas samples above/near the SMT at the nonhydrate-bearing sites are affected by the biogenic CH_4 with enriched ^{12}C; they indicate biogenic or thermogenic/biogenic mixed sources. The thermogenic gases below the SMT at ARAON Mounds have high C_1/C_{2+} ratios (>300), much higher than those of normal thermogenic gases in offshore shallow sediments (<100), due to postgenetic processes during migration.

The carbon isotopic fractionation ($\varepsilon_c = \delta^{13}C_{CO2} - \delta^{13}C_{CH4}$) in HS samples of the background site and ARAON Mounds above the SMT are consistent with the biogenic gas range generated via microbial CO_2 reduction. However, ε_c below the SMT is anomalously low (13–42‰) and is higher at the hydrate-bearing sites than at the nonhydrate-bearing sites. We postulate that this low ε_c is explained by the two-phase fluid transport model of Kim et al. (2012) and that gas hydrates highly influence this value. We suggest that ε_c can be used as a powerful geochemical proxy for the upward gas migration and gas hydrate occurrence in shallow marine sediment systems.

1. Introduction

A recent assessment of the stored carbon in the Arctic region indicated a mass of 1,000–2,000 Pg (10^{15} g) (McGuire et al., 2009). The organic carbon transported and buried in the Arctic Ocean through geological time can be used as a substrate to generate methane (CH_4) by microbial degradation through methanogenesis typically below ~80 °C or by thermal cracking at higher temperatures (Wilhelms et al., 2001;

* Corresponding author.
E-mail address: save@kigam.re.kr (J.-H. Kim).
[1] J.-H.K. and A.H. equally contributed to this work as co-first authors.

https://doi.org/10.1016/j.jngse.2020.103223
Received 7 December 2019; Received in revised form 12 February 2020; Accepted 17 February 2020
Available online 21 February 2020
1875-5100/

Stolper et al., 2014). Recently, in the Eastern Siberian Arctic shelf and offshore Svalbard, many CH_4 emissions from the seafloor to the water and/or atmosphere have been observed during geophysical surveys, which resulted in anomalously high CH_4 contents relative to that of the global mean ocean (Shakhova et al., 2005, 2010; Westbrook et al., 2009; Hong et al., 2017). This CH_4 release in the Arctic Ocean is principally derived from submarine permafrost degradation containing perennially frozen CH_4 produced via microbial or thermogenic pathways and gas hydrates, ice-like form of CH_4 (e.g., Dlugokencky et al., 2009; Kerr, 2010), which are stable under high-pressure and low-temperature conditions. CH_4 is usually a powerful greenhouse gas on Earth, whose warming effect is 28 times higher than that of CO_2 (IPCC, 2013; Mau et al., 2017). The CH_4 released from the seafloor to the water and/or atmosphere in the Arctic Ocean will continuously enhance global warming in the future. It will also trigger an increase in submarine permafrost thawing and gas hydrate dissociation in this region. Indeed, Hong et al. (2017) have suggested a high potential of Arctic gas hydrate dissociation if the seawater temperature will increase two degrees due to global warming during the next century.

The presence of gas hydrate has been reported in the Arctic Ocean, including mud volcanoes in the Beaufort Sea, Barents Sea, and offshore Svalbard, where access is not easily attained without ice-breaking vessels (Pape et al., 2011; Paull et al., 2015; Hong et al., 2017). The properties of pore water and gas are very sensitive to the gas flux and gas hydrate formation and dissociation. Therefore, the geochemistry of pore water and gas has been valuable to understand the characteristics of gas hydrate as well as gas seepage in the marine environment of the Arctic Ocean. In contrast, a few gas and pore water chemistry studies have focused on their origin and diagenesis in connection with gas seepage and gas hydrate in the Arctic Ocean (Coffin et al., 2013; Paull et al., 2015; Hong et al., 2017, 2018; Pape et al., 2011). It appears that the presence of gas hydrate and the related gas and pore water geochemistry in the central regions of the Arctic Ocean with thick sea ice have not yet been reported.

During the ARA07C Expedition in 2016 onboard Ice-breaking Research Vessel (*IBRV*) ARAON, gas hydrates were first discovered in a gravity core (GC) (<3 m in length) from the mound site (Site ARA07C-St 13; Fig. 1; Table 1) located at a water depth exceeding 600 m in the Chukchi Sea under heavy sea ice conditions. Here, we first report the compositional and isotopic properties of gas hydrates and dissolved gases (the headspace (HS) and void gases) as well as pore water properties in the core sediments from the Chukchi Sea acquired during both the ARA07C and ARA09C Expeditions. To date, there have been no studies on the gas sources and postgenetic processes that affect many gas properties during upward gas migration in the study area. In addition, the influence of the gas hydrate observed during upward gas migration on the gas chemistry of shallow sediments remains unclear. Therefore, the main aim of this study is to clarify the gas origin and postgenetic diagenesis at the hydrate- and nonhydrate-bearing sites in the Chukchi Sea and to investigate the influence of gas hydrate formation related to

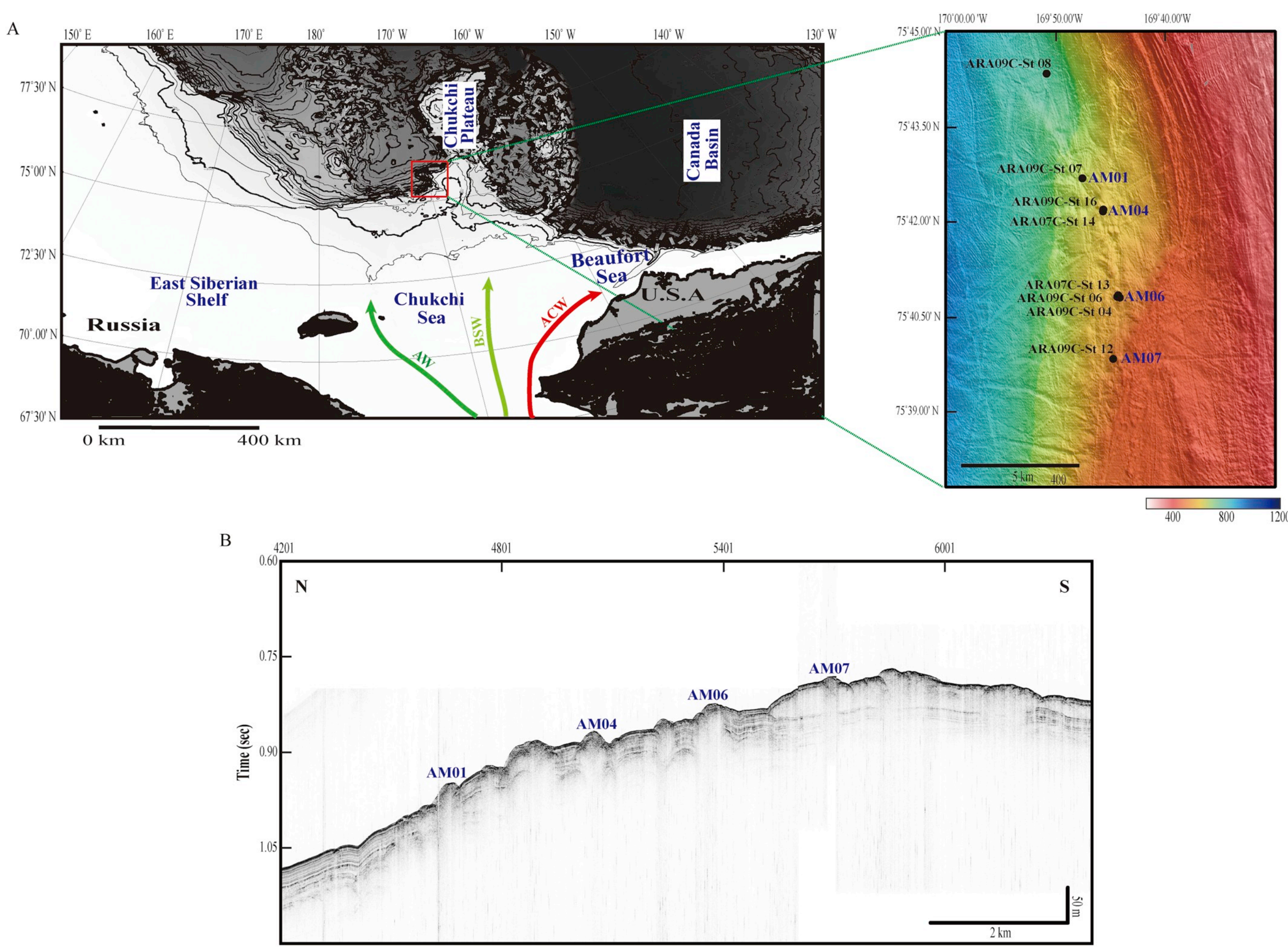

Fig. 1. A) Major physiographic feature, general physical oceanographic circulation, and multibeam result of the study area during the ARA07C and ARA09C Expeditions. Anadyr Waters (AW) shown in dark green arrow, Bering Shelf Waters (BSW) in light green arrow, and Alaska Coastal Waters (ACS) in red arrow. B) Subbottom profiles images of the ARAON Mounds (AM) surveyed during the ARA09C Expedition.

Table 1
Summaries of location, water depth, total core length, and depth of the SMT in each site from the ARA07C and ARA09C Expeditions.

Site	Latitude (N)	Longitude (W)	ARAON Mound number	Water depth (m)	Total core length (m)	Depth of the SMT (mbsf)	Remarks
ARA09C-St 08	75° 44.385′	169° 51.268′		815	5.28	—	Background
ARA07C-St 13	75° 40.799′	169° 44.192′	AM06	610	2.35	1.3	Mound structure/Gas hydrate and authigenic carbonate found
ARA09C-St 06	75° 40.840′	169° 44.195′		609	2.60	<0.2	
ARA09C-St 04	75° 40.793′	169° 44.210′		605	2.21	1.2	Mound structure/ Authigenic carbonate found
ARA07C-St 14	75° 42.201′	169° 45.552′	AM04	653	1.61	0.9	Mound structure/Gas hydrate and authigenic carbonate found
ARA09C-St 16	75° 42.204′	169° 45.649′		662	2.50	<0.1	
ARA09C-St 07	75° 42.717′	169° 47.684′	AM01	699	4.51	3.3	Mound structure/ Authigenic carbonate found
ARA09C-St 12	75° 39.822′	169° 44.458′	AM07	588	2.64	2.1	

* —: not reach.

upward gas migration. To achieve this aim, we combined and interpreted gas compositional and isotopic data with pore water and Rock-Eval pyrolysis data. The findings will improve our understanding of CH_4 behavior during migration from deep-seated sediments to the seafloor and the carbon cycles in the Arctic area. In addition, this study provides complementary gas and pore water data for the Arctic Ocean to predict future global warming on a global scale.

2. Study area

The Chukchi Sea, one of the largest marginal seas in the Arctic Ocean, extends from 66°N in the south to the edge of the Arctic Basin in the north, covering an area of 620,000 km^2 (Jakobsson, 2002). In this sea, the Chukchi Shelf encompasses the shallow continental margin north of Chukotka and Alaska is less than 50 m depth in the south to 450–750 m depth at the shelf break near the northward extension known as the Chukchi Rise. The Chukchi Borderland is an adjacent fragment of continental crust extending north into the Canada Basin of the Arctic Ocean (Grantz et al., 1998), which incorporates the Northwind Ridge and the Chukchi Plateau (Fig. 1).

Water masses flow across the Chukchi Sea along three main pathways: 1) the saline (>32.5‰) and nutrient-rich Anadyr Waters ($NO_3^- \geq$ 20 μM), 2) the relatively warm, fresher (<31.8‰) and nutrient-poor Alaska Coastal Waters, and 3) the Bering Shelf Waters in the central channel with moderate nutrient and salinity values (31.8–32.5‰) (Grebmeier et al., 1988; Woodgate and Aagaard, 2005; Weingartner et al., 2005; Hunt et al., 2013).

Ice sheets are critical factors for interpreting the paleoclimate and paleoceanography in the Chukchi Sea through geological time. The glaciogenic submarine landforms in the Chukchi Borderland have been primarily related to ice arriving from the Laurentide ice sheets possibly with local small ice caps on the Chukchi Plateau, and there has been a lack of terrestrial evidence for large-scale ice grounding on Wrangel Island, at least in the Late Pleistocene (Brigham-Grette et al., 2001; Gualtieri et al., 2005; Jakobsson et al., 2005, 2010; Polyak et al., 2007), indicating that the Chukchi Sea coast was free of large ice sheets. However, widespread scouring by a large ~1 km thick Arctic ice shelf during recent glacial periods has recently been reported (Polyak et al., 2001; Niessen et al., 2013), suggesting that Arctic ice sheets had still been influenced along the Arctic continental margins during the Last Glacial Maximum (LGM).

The study area in the Chukchi Sea has a relatively gentle slope (approximately 2°) with a >3 km wide terrace based on multibeam data, and eight mound structures have been observed along the edge of the terrace at a water depth between 568 m and 704 m in sub-bottom profiler (SBP) images (Fig. 1; Jin and Shipboard Scientific Party, 2019). These mounds are named ARAON Mound 01 to 08 (AM01 to AM08) from northwest to southeast and are approximately 10 m higher than the surrounding seafloor and 200–700 m wide. In addition, SBP images reveal that the acoustic facies, stratigraphy, and structure of the subsurface are different at each ARAON Mound because of the different sequences of notably thick facies interbedded in the stratified facies (Jin and Shipboard Scientific Party, 2019). In terms of acoustic characteristics and tectonics, the ARAON Mounds seem to have formed in association with basin bounding faults through the prolonged seepage active at this stage (Jin and Shipboard Scientific Party, 2019).

3. Materials and methods

3.1. Materials

During the ARA07C Expedition in 2016, two GCs were collected at Sites ARA07C-St 13 and ARA07C-St 14, located at AM06 and AM04, respectively (Fig. 1; Table 1). We revisited the ARAON Mounds in 2018 and obtained five GCs from AM01 (Site ARA09C-St 07), AM04 (Site ARA09C-St 16), AM06 (Sites ARA09C-St 06 and ARA09C-St 04), and AM07 (Site ARA09C-St 12). In addition, one GC was collected at Site ARA09C-St 08 as a background site, where a mound structure had not been observed in SBP images. The length of all GCs is shorter than 6 m (Fig. 1; Table 1).

During both the ARA07C and ARA09C Expeditions, void gas (VG) was sampled from the cores by piercing the liner with a 60 ml syringe immediately after core retrieval. This sample was transferred to a 60 ml serum vial filled with a saturated NaCl solution. For HS gas analysis, during the ARA07C Expedition, a 3 ml sediment sample was collected with a cut-off 5 ml plastic syringe from the freshly exposed end of each core section and extruded into a 2 ml glass serum vial. Two milliliters of saturated NaCl was added to each vial, which was then sealed with a 20 mm thick septum and a metal crimp cap. In contrast, during the ARA09C Expedition, 10 ml of sediment was collected for HS gas analysis from each split GC sample at certain intervals from 20 to 150 cm using a cut-off 5 ml plastic syringe. The sediment was placed in a 25 ml glass vial, after which a mixed solution consisting of 9.7 ml saturated saline water and 0.3 ml 50% benzalkonium chloride aqueous solution was added. Each vial was capped with a rubber septum and sealed with an aluminum cap, and then the HS, which consisted of air, was replaced with helium. Hydrate-bound gas (BG) samples were collected at three hydrate-bearing sites (ARA07C-St 13, ARA09C-St 06, and ARA09C-St 16). Several gas hydrate pieces in each sampling depth were carefully removed the adhering sediments in surface to minimize contamination and dissociated within a 60 ml syringe. The BG samples were collected using the same method as was used for VG sampling.

Pore water was extracted with a Rhizon sampler from whole or split cores at ~10–60 cm intervals at room temperature on *IBRV* ARAON. The extracted pore water was collected in 25 ml acid-prewashed syringes and filtered through an in-line 0.20 μm disposable polytetrafluoroethylene filter. Pore water aliquots for cation analysis were transferred into acid-prewashed high-density polyethylene (HDPE) bottles (~2–4 ml) and acidified with 20 μl ultrapure HNO_3. These samples were stored at approximately 4 °C in a refrigerator until further analysis.

At Sites ARA07C-St 13 and ARA07C-St 14, bulk sediment samples were continuously collected, and the samples were freeze-dried for 24 h. The dried samples were ground and homogenized in an agate mortar. Aliquots of the powdered samples were used for Rock-Eval analysis.

3.2. Gas analysis

HS gas was extracted during the ARA07C Expedition by heating the sediment samples at 60 °C for 30 min at the Korea Institute of Geosciences and Mineral Recourses, following the procedure described by Pimmel and Claypool (2001). In the experiments, the HS, VG, and BG samples were injected into an Agilent Technologies 7890A gas chromatograph with both a flame ionization detector (FID) and a thermal conductivity detector (TCD) to analyze the hydrocarbon composition (C_1–C_6) and CO_2. The reproducibility was less than 5% based on repeated standard analyses. The stable carbon ($\delta^{13}C_{CH4}$, $\delta^{13}C_{C2H6}$, and $\delta^{13}C_{CO2}$) and hydrogen (δD_{CH4}) isotopic ratios in the gas samples collected during the ARA07C Expedition were obtained using an isotope-ratio gas chromatograph-mass spectrometer at Isotech, Champaign, IL. The stable carbon and hydrogen isotope values are reported in the conventional δ notation in per mil (‰) relative to Vienna-Pee Dee Belemnite (V-PDB) and Vienna Standard Mean Ocean Water (V-SMOW), respectively. The reproducibility was ±0.1‰ for carbon and ±2.0‰ for hydrogen.

The gas compositions of the HS, VG, and BG samples from the ARA09C Expedition were determined at the Kitami Institute of Technology using a Shimadzu GC-2014 with a packed column (Shimadzu Sunpak-S; 2 m length and 3 mm ID), a TCD for detecting CO_2 and high (>0.1%) C_1 concentrations, and an FID for detecting low (<0.1%) hydrocarbon (C_1–C_5) concentrations. The reproducibility of repeated standard analyses was less than 1.2% for each gas component. The $\delta^{13}C_{CH4}$, $\delta^{13}C_{C2H6}$, $\delta^{13}C_{CO2}$, and δD_{CH4} values in the HS, VG, and BG samples from this expedition were measured using a continuous-flow isotope-ratio mass spectrometer (CF-IRMS, DELTA V, Thermo Fisher Scientific, Waltham, MA, USA) coupled with a gas chromatograph (Trace GC Ultra, Thermo Fisher Scientific). The gas chromatograph was equipped with a Carboxen-1006 PLOT capillary column (with a 30 m length, 0.32 mm ID, and 15 μm film thickness; Sigma-Aldrich, St. Louis, MO, USA). For samples with low C_1 concentrations, a Sigma-Aldrich Carboxen-1010 PLOT capillary column (with a 30 m length, 0.3 mm ID, and 15 μm film thickness) was also used to distinguish air and C_1 components. The stable carbon and hydrogen isotope values are reported in the conventional δ notation in per mil (‰) relative to V-PDB and V-SMOW, respectively. The reproducibility was ±0.3‰ for $\delta^{13}C$ and 2.0‰ for δD.

3.3. Pore water analysis

The sulfate (SO_4^{2-}) in the pore water from the ARA07C and ARA09C Expeditions was analyzed by ion chromatography (IC) at the Korea Basic Science Institute (Dionex ICS-1100, Thermo Scientific) and the Kitami Institute of Technology (2707 plus Autosampler, 1525 Binary HPLC Pump, and 432 Conductivity Detector, Nihon Waters K.K., Japan), respectively. IAPSO standard seawater was repeatedly analyzed to verify the analytical quality of the instruments, and the analytical reproducibility was less than ±3%.

3.4. Rock-Eval analysis

Rock-Eval pyrolysis was performed at the Korea Institute of Geoscience and Mineral Resources using a Rock-Eval Turbo 6 (Vinci Technologies, France) to determine the hydrocarbon source-rock potential of the organic matter in sediments. The free and adsorbed hydrocarbons released from a sample during programmed heating were recorded as the first peak in a pyrogram (S_1) at a low temperature (300 °C). The second peak (S_2) in the pyrogram represents the hydrocarbons released during kerogen cracking when the sample was heated from 300 to 550 °C. The temperature when the maximum S_2 peak is attained is defined as T_{max}. CO_2, which is shown as the third peak (S_3) in the program, was also generated due to kerogen degradation. When these components are normalized to the organic carbon content, the S_2 peak becomes the hydrogen index (HI; $S_2 \times 100$/TOC), and the S_3 peak becomes the oxygen index (OI; $S_3 \times 100$/TOC). The total organic carbon (TOC) is measured by summing the pyrolyzed carbon (PC) and residual carbon (RC) fractions (Arthur et al., 1998; Lafargue et al., 1998).

4. Results

4.1. Dissolved SO_4^{2-} profile

The dissolved SO_4^{2-} profiles in pore water are largely classified into three trends (Fig. 2; Supplementary Table 1). The first trend observed at Site ARA09C-St 08 (the background site) is a near-linear decrease from the seawater value (~30 mM) near the seafloor to ~24 mM at 5 m below the seafloor (mbsf). This suggests that the penetration depth at Site ARA09C-St 08 does not reach the sulfate-methane transition (SMT) depth. The second trend exhibits a relatively constant value or a gradually decreasing trend with the depth at shallow depths and then sharply decreases with the depth, and the SMT depth is reached. Below the SMT depth, the dissolved SO_4^{2-} concentration is a relatively constant value or a gradually decreasing value (>27 mM) with the depth. This trend has been observed at Sites ARA07C-St 13, ARA07C-St 14, ARA09C-St 04, ARA09C-St 07, and ARA09C-St 12. Gas hydrates were first encountered at the bottom of Site ARA07C-St 13 during the ARA07C Expedition, whereas they were not observed at the other sites (Jin and Shipboard Scientific Party, 2017, 2019). The last trend exhibits a very low SO_4^{2-} concentration along the entire core length (<2.0 mM) without any distinct trend, as observed at Sites ARA09C-St 06 and ARA09C-St 16. In contrast, many gas hydrates were discovered at shallow depths (<0.5 mbsf) at both sites during the ARA09C Expedition (Jin and Shipboard Scientific Party, 2019), suggesting that the SMT depth is probably very shallow at these two sites (<0.5 mbsf). Therefore, the dissolved SO_4^{2-} trends at Sites ARA09C-St 06 and ARA09C-St 16 are likely to be caused by ambient seawater contamination during coring, because seawater can enter GC sediments due to gas hydrate dissociation.

4.2. Gas composition properties

The gas composition properties of the HS, VG, and BG samples are presented in Fig. 2 and Supplementary Table 2. The CH_4 concentration in the HS samples from Sites ARA09C-St 04, ARA09C-St 07, and ARA09C-St 12 was the lowest (<120 ppm vol.) near the seafloor and increased sharply below the SMT depth (>10,000 ppm vol.). In contrast, the CH_4 concentration in the HS samples from the background site (ARA09C-St 08) was generally lower, ranging from 13 to 3,300 ppm vol. The ethane (C_2H_6) concentration also increased below the SMT depth at Sites ARA09C-St 04, ARA09C-St 07, and ARA09C-St 12 (>30 ppm vol.). At Sites ARA09C-St 06 and ARA09C-St 16, all CH_4 concentrations in the HS samples were high (>19,000 ppm vol.), which is caused by gas hydrate dissociation. The C_1/C_{2+} ratios in the HS samples below the SMT depth at the ARAON Mounds generally exceeded 300 because CH_4 is a predominant hydrocarbon gas and C_{2+} is a tracer (Supplementary Table 2). The C_1/C_{2+} ratio at Site ARA09C-St 08 ranged from 20 to 880,

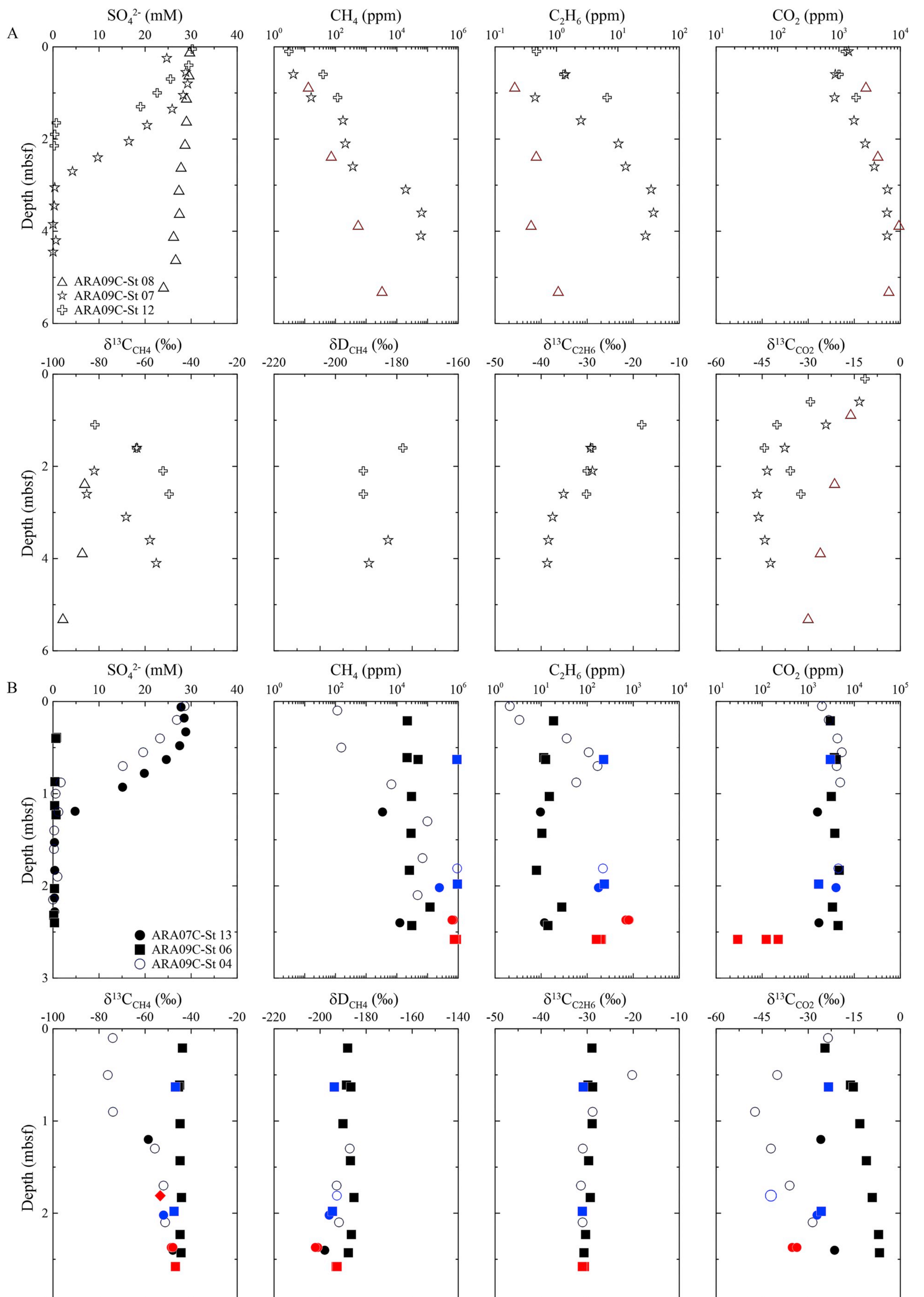
A
B
SO_4^{2-} (mM)
CH_4 (ppm)
C_2H_6 (ppm)
CO_2 (ppm)
Depth (mbsf)
$\delta^{13}C_{CH4}$ (‰)
δD_{CH4} (‰)
$\delta^{13}C_{C2H6}$ (‰)
$\delta^{13}C_{CO2}$ (‰)
ARA09C-St 08
ARA09C-St 07
ARA09C-St 12
ARA07C-St 13
ARA09C-St 06
ARA09C-St 04

Fig. 2. Downcore profiles of dissolved sulfate (SO_4^{2-}) in pore water, CH_4, C_2H_6, CO_2, $\delta^{13}C_{CH4}$, δD_{CH4}, $\delta^{13}C_{C2H6}$, and $\delta^{13}C_{CO2}$ of headspace (HS) gases, void gases (VG), and hydrate-bound gases (BG) at A) Sites ARA09C-St 08 (background site; open triangles) ARA09C-St 07 (AM01; open stars), and ARA09C-St 12 (AM07; open crosses), B) Sites ARA07C-St 13 (closed circles), ARA09C-St 06 (closed squares), and ARA09C-St 04 (open circles) from the AM06, and C) Sites ARA09C-St 16 (closed diamonds) and ARA07C-St 14 (open diamonds) from the AM04. HS shown in black open symbols at the nonhydrate-bearing sites whereas HS in black closed symbols, VG in blue closed symbols, and BG in red closed symbols at the hydrate-bearing sites.

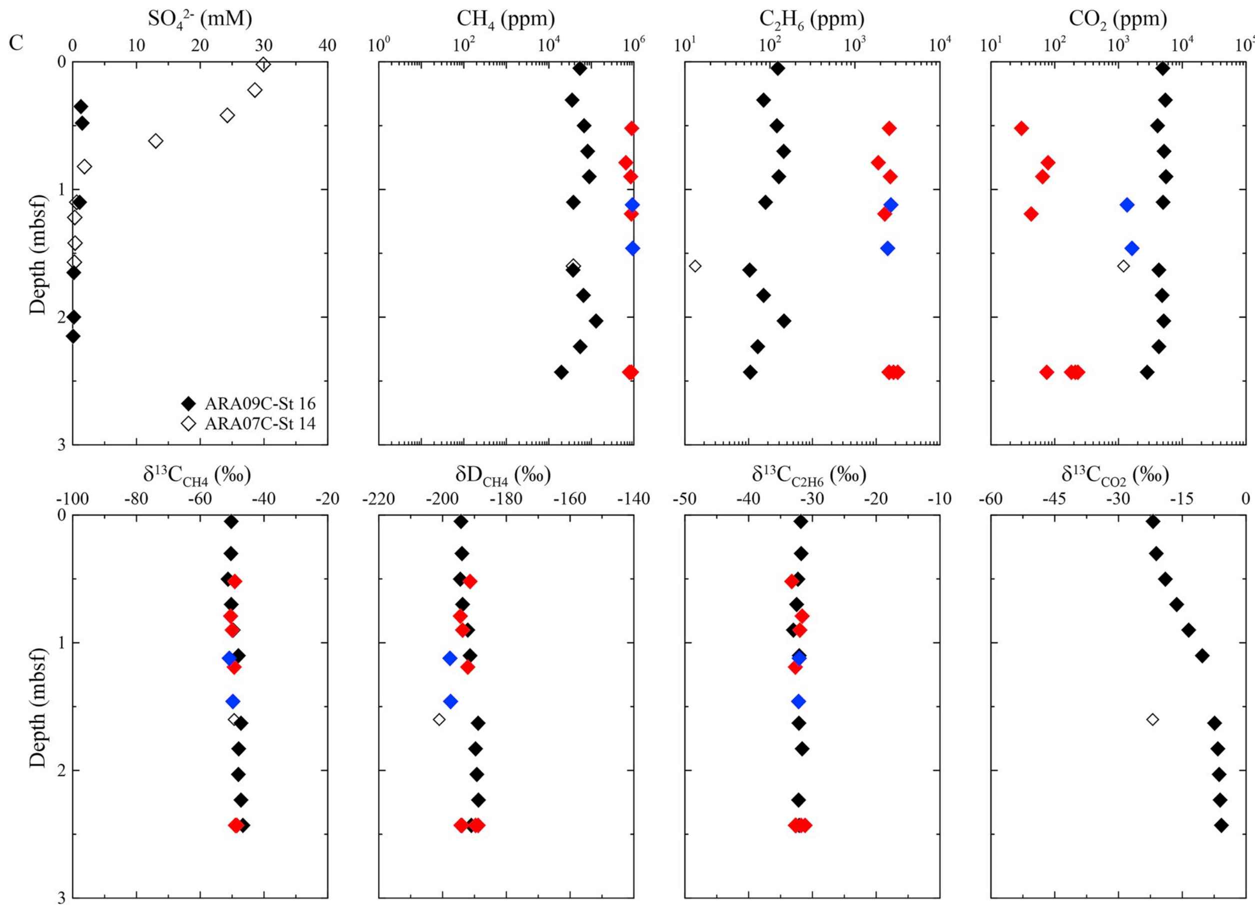

Fig. 2. (*continued*).

and was a lower value observed at shallow depths (<2.7 mbsf) (Supplementary Table 2). The hydrocarbon gases in all VG and BG samples from the ARAON Mounds were mainly composed of CH_4 with little C_{2+}, while C_{4+} was not detected. As a result, the C_1/C_{2+} ratio in all VG and BG samples is also higher than 300 (Supplementary Table 2). The CO_2 profiles in the HS samples were similar between the ARAON Mounds and background sites. Interestingly, the CO_2 concentration in the HS and VG samples was higher than that in the BG samples from the ARAON Mounds (Fig. 2: Supplementary Table 2).

4.3. Gas isotopic properties

The carbon and hydrogen isotopic signatures of the hydrocarbon gases ($\delta^{13}C_{CH4}$, $\delta^{13}C_{C2H6}$, and δD_{CH4}) and carbon dioxide ($\delta^{13}C_{CO2}$) in the HS, VG, and BG samples are shown in Fig. 2 and Supplementary Table 2. The minimum $\delta^{13}C_{CH4}$ value in the HS samples generally occurred near the SMT depth at Sites ARA09C-St 04, ARA09C-St 07, and ARA09C-St 12. The $\delta^{13}C_{C2H6}$ value at these sites ranged from −42.1‰ to −18.1‰, which generally decreases with depth. The minimum $\delta^{13}C_{CO2}$ value in the HS samples also occurred near the SMT at these sites. The $\delta^{13}C_{CH4}$ and $\delta^{13}C_{CO2}$ values in the HS samples from Sites ARA09C-St 06 and ARA09C-St 16 were significantly enriched ($\delta^{13}C_{CH4} > -51$‰ and $\delta^{13}C_{CO2} > -27$‰) across the entire coring depth compared to those in the HS samples from the nonhydrate-bearing sites. Both the $\delta^{13}C_{CH4}$ and $\delta^{13}C_{CO2}$ values at Site ARA09C-St 08 decreased with the depth. The δD_{CH4} value in the HS samples from all sites had a relatively constant range from −200‰ to −180‰ and did not show a distinct trend.

The $\delta^{13}C_{CH4}$, $\delta^{13}C_{C2H6}$, $\delta^{13}C_{CO2}$, and δD_{CH4} values were not notably different between the VG and BG samples from Sites ARA07C-St 13, ARA09C-St 06, and ARA09C-St 16. In addition, these values were nearly the same as those in the HS samples collected at similar sampling depths (Fig. 2: Supplementary Table 2).

4.4. Rock-Eval analysis

Most TOC contents at Sites ARA07C-St 13 and ARA07C-St 14 were higher than 0.5 wt%, varying between 0.44 wt% and 1.76 wt% (n = 29; average = 0.85 ± 0.39 wt%) and between 0.58 wt% and 1.18 wt% (n = 14; average = 0.81 ± 0.29 wt%), respectively (Supplementary Table 3). All measured HI and T_{max} values of the sedimentary organic matter at Sites ARA07C-St 13 and ARA07C-St 14 were lower than 100 mgHC/gTOC and 435 °C, respectively, and these values were located along the Type III evolution path, indicating that the organic matter was thermally immature (Fig. 3: Supplementary Table 3). These results suggest that the organic matter at Sites ARA07C-St 13 and ARA07C-St 14 originates from terrigenous organic matter and cannot generate hydrocarbons in situ (Tissot and Welte, 1984; Nali et al., 2000).

5. Discussion

5.1. Sulfate-methane transition (SMT)

The organic matter in a marine system is generally decomposed by particulate organic matter sulfate reduction (POCSR; $2CH_2O + SO_4^{2-} \rightarrow 2HCO_3^- + H_2S$) above the SMT and by methanogenesis (ME) via acetate fermentation or CO_2 reduction below the SMT. Near the SMT, organic matter is also degraded by the anaerobic oxidation of methane (AOM; $CH_4 + SO_4^{2-} \rightarrow HCO_3^- + HS^- + H_2O$) (Borowski et al., 1996). Because SMT is not reached at Site ARA09C-St 08 (Fig. 2; Supplementary Table 1), POCSR is the main organic matter degradation reaction. In contrast, SMT is occurred at the other sites near the ARAON Mounds (Fig. 2; Supplementary Table 1); thus, POCSR, AOM, and ME via CO_2 reduction sequentially degrade the organic matter in the sediment column with increasing depth from the seafloor. These results are clearly supported by the along-core profile of the CH_4 concentration at each site (Fig. 2: Supplementary Table 1).

A concave-up dissolved SO_4^{2-} profile was observed in the pore water from Sites ARA07C-St 13, ARA07C-St 14, ARA09C-St 04, ARA09C-St 07, and ARA09C-St 12, similar to the second dissolved SO_4^{2-} trend at a shallow SMT depth (≤3.3 mbsf) (Fig. 2). Similar SO_4^{2-} profiles have been reported in other regions, such as the Northern Congo Fan, the Argentine Basin, the Arabian Sea, and the Gulf of Mexico (Zabel and Schulz, 2001; Hensen et al., 2003; Ussler and Paull, 2008; Nothen and Kasten, 2011; Kasten et al., 2012; Fischer et al., 2013; Wilson et al., 2014). Ussler and Paull (2008) revealed that this SO_4^{2-} profile indicates a diffusive unsteady state and SMT migration toward the seawater-sediment interface due to an increasing gas flux. Hence, our observed SO_4^{2-} profile at the ARAON Mounds is another example of this interpretation. We postulate that the gas flux at each site of the ARAON Mounds is a critical factor influencing the composition and isotopic properties of the pore water and gas.

5.2. Gas source and migration process

Hydrocarbon sources are commonly identified by the composition and isotopic characteristics of gases (Bernard et al., 1976; Whiticar et al., 1986; Schoell, 1988; Whiticar, 1999; Pape et al., 2010; Kim et al., 2012, 2013). The hydrocarbon gas generated by microbial CO_2 reduction mainly consists of methane (C_1) and traces of ethane (C_2) and propane (C_3), resulting in relatively high C_1/C_{2+} ratios (commonly > 1,000). In contrast, thermogenic gases are commonly enriched in C_{2+} and thus exhibit low C_1/C_{2+} ratios (<100) (Whiticar et al., 1986; Whiticar, 1999; Milkov et al., 2005; Pape et al., 2010; Kim et al., 2011, 2012, 2013). In all HS, VG, and BG samples from the ARAON Mounds, CH_4 dominates the composition with $C_1/C_{2+} > 300$ (Supplementary Table 2), which likely suggests that CH_4 is predominantly of microbial origin. On the other hand, the Bernard diagram displaying the relationship between $\delta^{13}C_{CH4}$ and the C_1/C_{2+} ratio deviates from this finding. In this diagram, most HS and all VG and BG samples from the ARAON Mounds are located outside both the microbial and thermogenic regions, implying that the CH_4 from the ARAON Mounds does not simply come from a microbial or thermogenic source (Fig. 4A).

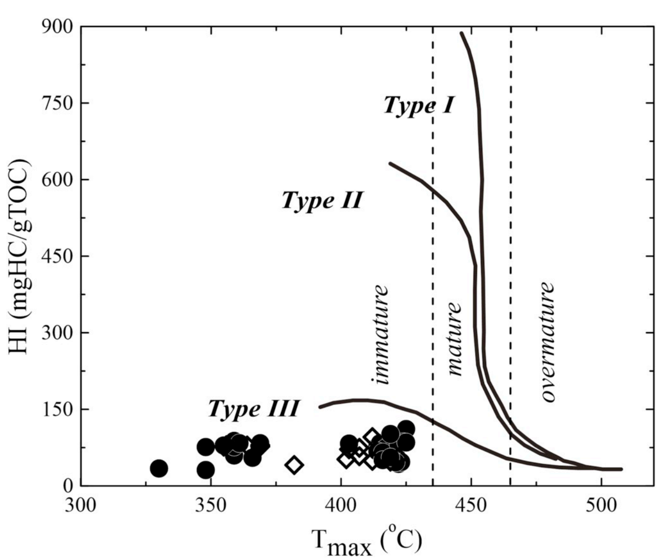

Fig. 3. Scatter plot of T_{max} versus HI in organic matters of sediments from Sites ARA07C-St 13 (closed circles) and ARA07C-St 14 (open diamonds).

As shown in Fig. 4B, the diagram of $\delta^{13}C_{CH4}$ and δD_{CH4} is plotted to clarify the CH_4 source at the ARAON Mounds since the $\delta^{13}C_{CH4}$ and δD_{CH4} values have indicated remarkably different gas origins; $\delta^{13}C_{CH4}$ and δD_{CH4} typically range from −110‰ to −50‰ and from −400‰ to −100‰, respectively, indicating a microbial CH_4 source, whereas they vary from −50‰ to −20‰ and from −275‰ to −50‰, respectively, indicating a thermogenic CH_4 source (Whiticar, 1999). All $\delta^{13}C_{CH4}$ and δD_{CH4} values in the VG and BG samples from the ARAON Mounds suggest a thermogenic CH_4 origin, implying that CH_4 is mainly derived from an allochthonous thermogenic source (deep-seated sediments; see Section 5.3). BG gases with a thermogenic CH_4 source at shallow depths (<6 mbsf) have also been reported in the Gulf of Mexico, offshore Vancouver, and offshore Svalbard, where a high gas flux is identified at the seafloor (Milkov, 2005; Plaza-Faverola et al., 2017). In contrast, the HS samples from the ARAON Mounds are largely classified into three regions with the depth: 1) a biogenic CH_4 source at Site ARA07C-St 12 (~1.6 mbsf), 2) a mixture of biogenic and thermogenic CH_4 above/near the SMT at Sites ARA09C-St 04 (~1.3 mbsf) and ARA09C-St 07, and 3) a thermogenic CH_4 origin below the SMT at Sites ARA07C-St 13, ARA07C-St 14, ARA09C-St 04 (>1.7 mbsf), ARA09C-St 06, ARA09C-St 12 (>2.1 mbsf), and ARA09C-St 16. Interestingly, most CH_4 in the HS samples from the hydrate-bearing sites (ARA07C-St 13, ARA09C-St 06, and ARA09C-St 16) only indicates a thermogenic source, while the source of the CH_4 collected at the nonhydrate-bearing sites ranges from a mixture of biogenic and thermogenic sources to a thermogenic source (ARA09C-St 04 and ARA09C-St 12) or from a biogenic to a thermogenic source (ARA09C-St 07) within a 1 m interval near the SMT. This suggests that the CH_4 source, which dominates the gas composition, rapidly changed vertically and horizontally at the ARAON Mounds, first reported in the Chukchi Sea. The ARAON Mounds have a very shallow SMT (≤3.3 mbsf), and gas hydrates have been discovered near the seafloor, which are consistent with the unique characteristics of the areas with high upward gas fluxes observed in the Ulleung Basin, offshore Oregon, Gulf of Mexico, offshore Vancouver, and offshore Svalbard (Milkov, 2005; Kim et al., 2011, 2012; Plaza-Faverola et al., 2017). We determined a thermogenic CH_4 origin in the HS samples, including the BG and VG samples collected below the SMT at all ARAON Mounds sites, whereas the gas composition and isotopic properties of the HS samples from the background site indicate biogenic CH_4. Therefore, the thermogenic CH_4 signatures observed at the ARAON Mounds are attributed to gas migration from deep-seated sediments (Fig. 5). Since the SMT depth is shallower at the hydrate-bearing sites than that at the nonhydrate-bearing sites of the ARAON Mounds, the upward gas flux to the seafloor at the former is higher than that at the latter (Borowski et al., 1996), which leads to a thermogenic CH_4 source close to the seafloor (Fig. 5). In addition, the HS samples from the hydrate-bearing sites are potentially affected by gas hydrate dissociation during coring because they occur at a very shallow depth (<0.5 mbsf) with similar $\delta^{13}C_{CH4}$ values to those of deep-sourced thermogenic CH_4. Overall, the CH_4 in all HS samples from the hydrate-bearing sites at the ARAON Mounds is thermogenic.

Although the δD_{CH4} data from the HS samples are limited above the SMT at the ARAON Mounds, the $\delta^{13}C_{CH4}$ value in the HS samples from Sites ARA09C-St 04, ARA09C-St 07, and ARA09C-St 12 reflected a

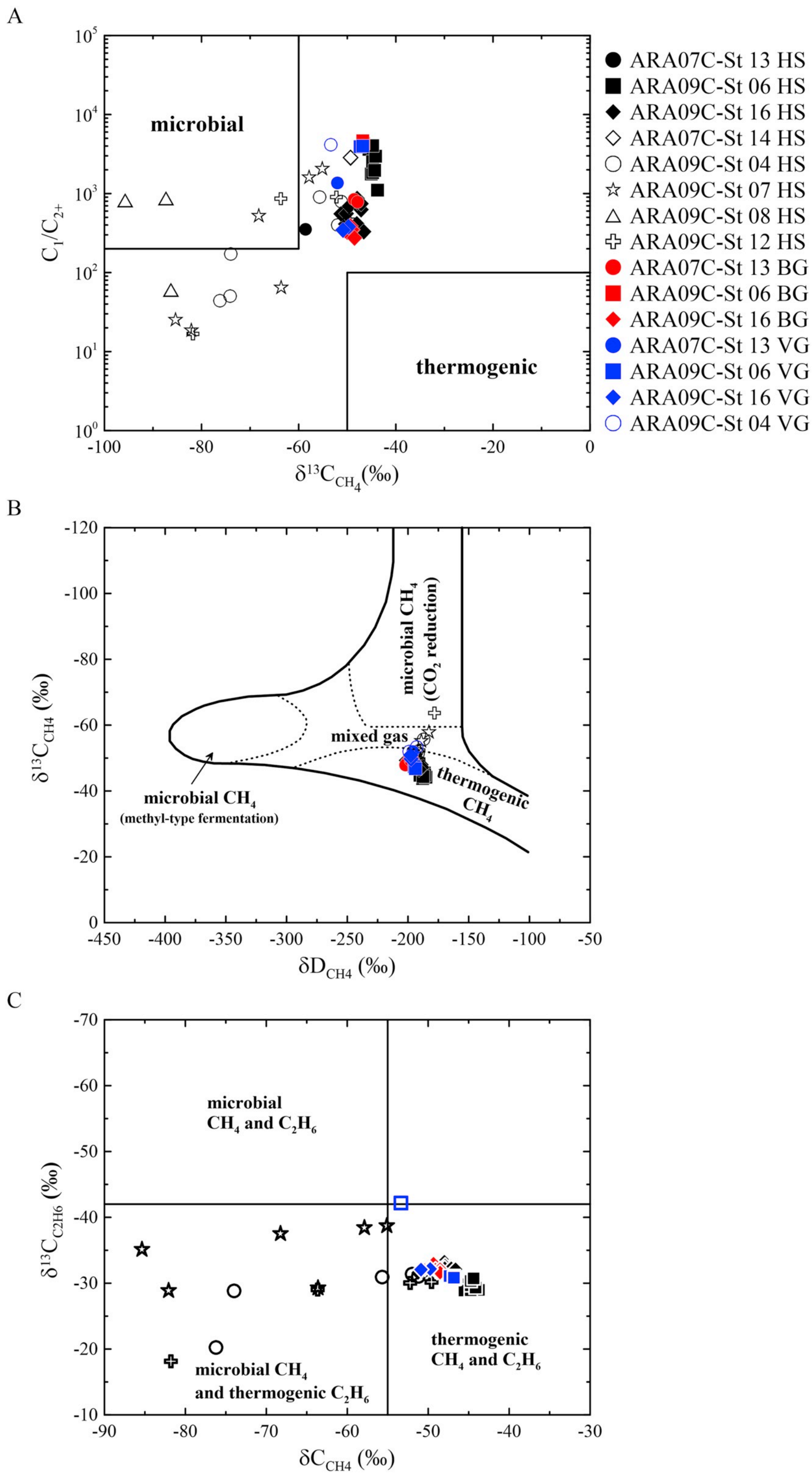

Fig. 4. A) Bernard diagram (after Bernard et al., 1978), which combines molecular and isotopic information to group gases into microbial and thermogenic fields. B) $\delta^{13}C_{CH4}$ versus δD_{CH4} diagram indicating a microbial origin via CO_2 reduction, mixture origin between biogenic and thermogenic, and thermogenic origin for the methane in all gas samples from the study area (adapted from Whiticar, 1999). C) $\delta^{13}C_{C2H6}$ versus $\delta^{13}C_{CH4}$ of all gases samples from the ARAON Mounds (adapted from Milkov et al., 2005), showing the thermogenic $\delta^{13}C_{CH4}$ and both biogenic and thermogenic $\delta^{13}C_{CH4}$. HS shown in black open symbols at the nonhydrate-bearing sites whereas HS in black closed symbols, VG in blue closed symbols, and BG in red closed symbols at the hydrate-bearing sites.

biogenic source (<−60‰), which is evident for the generation of autochthonous biogenic CH_4 above the SMT. The various pore water and gas chemistry results clearly support the occurrence of the AOM reaction near the SMT at these sites. As a result, deep-sourced thermogenic CH_4 cannot be encountered above the SMT and in the water column because most of the migrated CH_4 is efficiently removed by the AOM reaction (Figs. 2 and 5). In addition, many methane-derived authigenic carbonates are observed within the core sediments from the nonhydrate and hydrate-bearing sites, and gas hydrates occur at the hydrate-bearing sites of the ARAON Mounds (Jin and Shipboard Scientific Party, 2017, 2019), which are likely to partly act as cap rock to prevent gas transport from the sediment column to the water column and/or the atmosphere. The biogenic CH_4 produced above the SMT can diffuse and mix with the thermogenic CH_4 near the SMT; thus, a mixed CH_4 source signal of

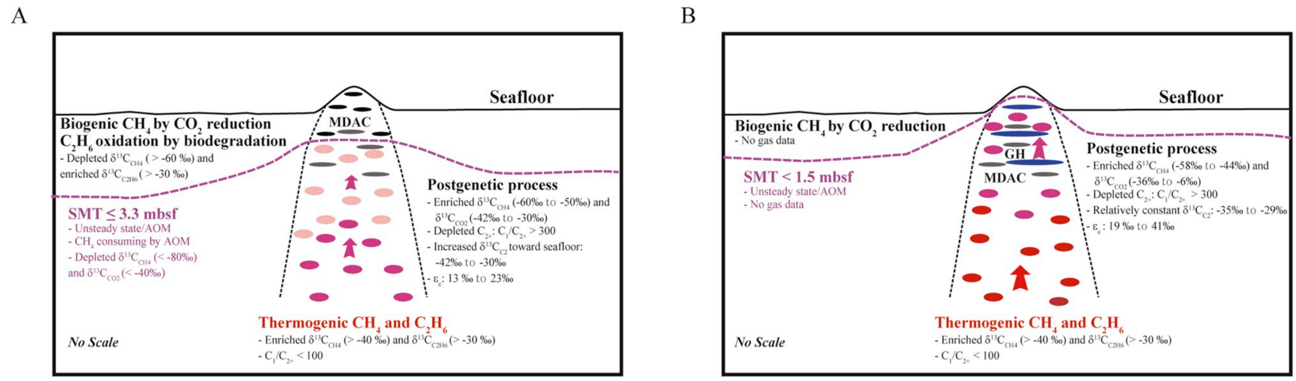

Fig. 5. Schematic diagram illustrating upward gas migration from the deep-seated sediments column at the A) nonhydrate-bearing and B) hydrate-bearing sites of the ARAON Mounds. The color change is the relative degree of the mixture between thermogenic and biogenic gas (red < dark pink < light pink) and the size of arrow is shown the relatively gas flux. Gas hydrate (GH) and methane-derived authigenic carbonate (MDAC) are displayed as blue circles and gray circles, respectively.

biogenic and thermogenic origins is detected above/near the SMT (Fig. 5). Furthermore, the dissolved SO_4^{2-} in the pore water and CH_4 do not have enough time to reach the steady state near the SMT due to the high gas flux. Therefore, the CH_4 source sharply changes at the nonhydrate-bearing sites of the ARAON Mounds with the depth; a biogenic source via CO_2 reduction above the SMT, a mixture of biogenic and thermogenic sources near the SMT, and mostly a thermogenic source below the SMT are observed in descending order. The diagram of the relationship between $\delta^{13}C_{CH4}$ and $\delta^{13}C_{C2H6}$ also supports this interpretation.

All $\delta^{13}C_{C2H6}$ values in the HS, VG, and BG samples from the ARAON Mounds are higher than −42‰ (Fig. 4C), indicating that the ethane predominantly originates from a thermogenic source (Milkov, 2005; Hachikubo et al., 2010). The maximum $\delta^{13}C_{C2H6}$ value is observed above the SMT, which will be discussed in Section 5.3. However, the $\delta^{13}C_{CH4}$ values indicated both biogenic and thermogenic sources. All $\delta^{13}C_{CH4}$ values in the HS, VG, and BG samples from Sites ARA07C-St 13, ARA07C-St 14, ARA09C-St 06, and ARA09C-St 16 predominantly indicate a thermogenic CH_4 source, while most HS samples from Sites ARA09C-St 04, ARA09C-St 07, and ARA09C-St 12 above/near the SMT and some HS samples collected at these sites below the SMT indicate a biogenic CH_4 source (Fig. 4C). These results also clearly imply that CH_4 is predominantly biogenic from the seafloor to the SMT, and then the gas source is quickly altered to a thermogenic source below the SMT at the nonhydrate-bearing sites of the ARAON Mounds.

5.3. Postgenetic process

The T_{max} values of the organic matter in the sediments at Sites ARA07C-St 13 and ARA07C-St 14 are located in the immature stage (<435 °C; Fig. 3 and Supplementary Table 3), which means that mostly microbial CH_4 is generated within the retrieved cores at these sites. In contrast, the measured isotopic signatures of CH_4 and C_2H_6 below the SMT at the ARAON Mounds clearly suggest a thermogenic source (Fig. 4). Overall, the hydrocarbon gas at the ARAON Mounds is not generated from autochthonous thermogenic sources but has migrated from the deeper sediment column to the seafloor through conduits.

Since the background geothermal gradient in the study area is 57 °C/km, which has been measured during the ARA09C Expedition (Jin and Shipboard Scientific Party, 2019), thermogenic hydrocarbon gas can be produced below at least > 1.0 km if thermal CH_4 generation begins with catagenesis defined in the temperature window from ~60 to 150 °C (Tissot and Welte, 1984; Sajgó, 2000). In the Chukchi Sea, many faults and fractures have been observed in deep seismic data (Hegewald and Jokat, 2013; Dove et al., 2014; Ilhan and Coakley, 2018), which function as conduits for gas migration from deeper sediment columns to the seafloor. Additionally, the prominent morphological characteristic of the study area includes mound structure formed by upward fluid flow and commonly found mass amounts of gas hydrates near the seafloor (e. g., Sassen et al., 1999; Suess et al., 1999; Paull et al., 2008; Waage et al., 2019). We postulate that, at the ARAON Mounds, deep-sourced thermogenic gas is upwardly transported through faults and/or fractures as conduits to the shallow sediment column, which can provide enough CH_4 to form mound structures and gas hydrates at the seafloor. This is consistent with the results from acoustic and tectonic approaches to analyze the ARAON Mounds (Jin and Shipboard Scientific Party, 2019).

Biogenic and thermogenic CH_4 can be mixed by diffusion and advective mixing. CH_4 undergoes transport-induced isotopic fractionation in a diffusion-dominated system, which leads to the preferential removal of the enriched $^{12}CH_4$. Consequently, the remaining CH_4 experiences $^{13}CH_4$ enrichment with a relatively lower molecular fraction (C_2/C_1; high C_1/C_2) (Pernaton et al., 1996; Prinzhofer and Pernaton, 1997; Whiticar, 1999). In contrast, when advective mixing of thermogenic and biogenic CH_4 progressively occurs, $\delta^{13}C_{CH4}$ and C_2/C_1 demonstrate a notable linearity (Fig. 6; Prinzhofer and Pernaton, 1997). Applying this approach to our data, the HS gases from Sites ARA09C-St 04, ARA09C-St 07, and ARA09C-St 12 at the ARAON Mounds do not display typical diffusion or a mixing line, whereas they generally follow the reversed mixing line, that is, the $\delta^{13}C_{CH4}$ values decrease with increasing C_2/C_1 (Fig. 6A and B). This trend has also been observed in Delaware Basin gases collected from 1,700 to 5,700 m below the surface, which accounts for the thermogenic trend based on the degree of thermal maturity (Stahl and Carey, 1975; Prinzhofer and Pernaton, 1997). The HS samples from Sites ARA09C-St 04, ARA09C-St 07, and ARA09C-St 12 at the ARAON Mounds also exhibit a good correlation between ($\delta^{13}C_{CH4}$ - $\delta^{13}C_{C2H6}$) and ln(C_1/C_2), which clearly indicates a thermogenic trend (Fig. 6C; Prinzhofer and Huc, 1995). The maturity of the organic matter and of the gas migrating upward from a deep-seated source toward the seafloor do not notably vary within the 6 m coring depth interval at the ARAON Mounds; however, this interpretation is overemphasized due to a lower C_2/C_1 (higher C_1/C_2). Overall, neither geochemical indicator can directly discriminate the upward gas migration mechanism at the ARAON Mounds. Since the dissolved SO_4^{2-} in the pore water does not reach the steady state near the SMT due to the high upward gas flux, advective mixing may be the preferential migration process for diffusion at the ARAON Mounds.

Thermogenic gas under catagenesis usually has a low C_1/C_{2+} ratio (<100) due to C_{2+} gas enrichment. Indeed, the BG gases at shallow depths in the Gulf of Mexico and offshore Vancouver, mainly derived from an allochthonous thermogenic source, have low C_1/C_{2+} ratios (mostly < 10). In contrast, the C_1/C_{2+} ratios in all gases from the ARAON Mounds are high (>300), which do not agree with the gas

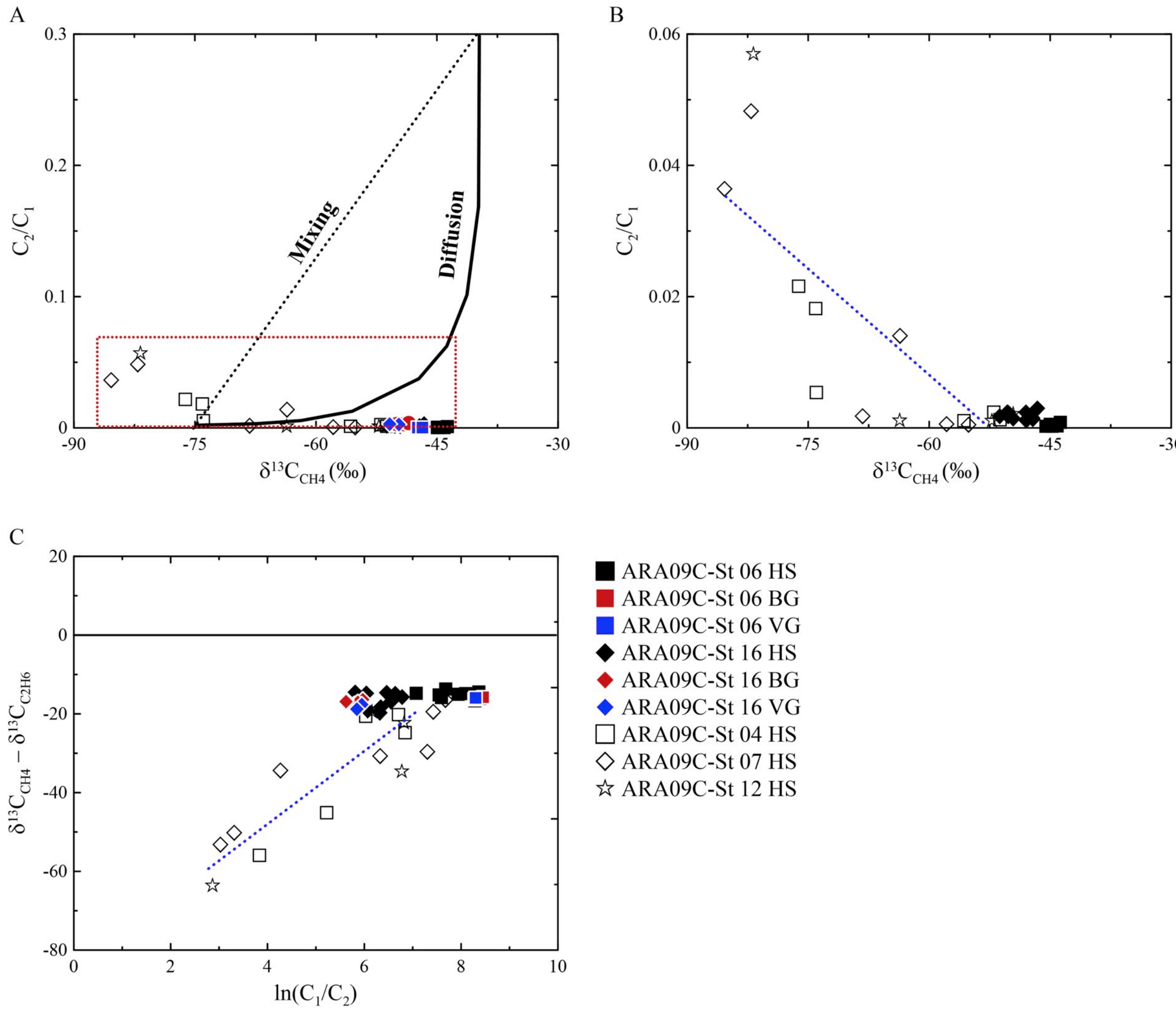

Fig. 6. Scatter plots of A) C_2/C_1 versus $\delta^{13}C_{CH4}$ of all gases from Sites ARA09C-St 06, ARA09C-St 16, ARA09C-St 04, ARA09C-St 07, and ARA09C-St 12, and B) C_2/C_1 versus $\delta^{13}C_{CH4}$ of HS gases from Sites ARA09C-St 06, ARA09C-St 16, ARA09C-St 04, ARA09C-St 07, and ARA09C-St 12 that is expanded the red dotted regions in panel A) (adapted from Prinzhofer and Pernaton, 1997). C) Scattering plot ($\delta^{13}C_{CH4}$ - $\delta^{13}C_{C2H6}$) versus $\ln(C_1/C_2)$ of all gases from Sites ARA09C-St 06, ARA09C-St 16, ARA09C-St 04, ARA09C-St 07, and ARA09C-St 12 (adapted from Prinzhofer and Huc, 1995). HS shown in black open symbols at the nonhydrate-bearing sites whereas HS in black closed symbols, VG in blue closed symbols, and BG in red closed symbols at the hydrate-bearing sites.

isotopic signatures of CH_4 and C_2H_6 implying a thermogenic source. Although the data set is limited, similar results to our observations have been reported for BG and HS samples from offshore Svalbard (Plaza--Faverola et al., 2017). One possibility for the high C_1/C_{2+} ratios at the ARAON Mounds is thermal cracking of C_{2+} gas. At a high thermal maturity (>150 °C; metagenesis), CH_4 is generated by thermal cracking of C_{2+} gas (Tissot and Welte, 1984; Sajgó, 2000), which leads to high C_1/C_{2+} ratios. However, the $\delta^{13}C_{CH4}$ values at the ARAON Mounds are much lower than those of the thermogenic gas produced by this reaction (>−30‰; Milkov and Etiope, 2018), and we exclude CH_4 generation via thermal cracking. There is another critical factor impacting the high C_1/C_{2+} ratios at the ARAON Mounds.

The composition and isotopic signatures of hydrocarbon gas can be affected by postgenetic processes, including physical (adsorption/desorption and diffusion in the gas or water phase) or chemical (bacterial and thermal alteration) processes (James and Burns, 1984; Prinzhofer and Pernaton, 1997). During hydrocarbon gas migration from deep-seated sediments toward the seafloor, longer-chain hydrocarbon gases are left behind (Schoell, 1984a,Schoell, 1984b; Price and Schoell, 1995), and microbial alteration continuously progresses. In this alteration, C_{2+} to C_1 in hydrocarbon gas are usually preferentially removed, and ^{13}C becomes enriched in the residual components (Fig. 5) (James and Burns, 1984). At the ARAON Mounds, $\delta^{13}C_{CH4}$ below the SMT has a relatively constant value ranging from −60‰ to −44‰ and becomes significantly depleted near the SMT by the mixing of the enriched ^{12}C with a microbial CH_4 source (Figs. 2 and 5), which is not consistent with ^{13}C enrichment in the residual CH_4. In contrast, the $\delta^{13}C_{C2H6}$ value in the HS samples, not significantly affected by the AOM reaction, indicates notable ^{13}C enrichment close to the SMT at the deeper sampling depths and reaches a maximum value at shallow depths above the SMT at the nonhydrate-bearing sites (ARA09C-St 04, ARA09C-St 07, and ARA09C-St 12). However, the HS samples from the hydrate-bearing sites have a relatively constant $\delta^{13}C_{C2H6}$ value, which is similar to those in the VG and BG samples due to the influence of gas hydrate dissociation (Figs. 2 and 5; Supplementary Table 2). The observed $\delta^{13}C_{C2H6}$ enrichment in the HS samples from the nonhydrate-bearing sites is evidence for the occurrence of microbial alteration of the hydrocarbon gases in an anoxic environment. Overall, the hydrocarbon gases at the ARAON Mounds significantly influence the microbial alteration during gas migration through geological time, which results in a high C_1/C_2 ratio with $\delta^{13}C_{C2H6}$ enrichment (Fig. 5).

5.4. Carbon isotopic fraction ratio

The carbon isotopic ratio differences of CO_2 and CH_4 ($\varepsilon_c = \delta^{13}C_{CO2}$ - $\delta^{13}C_{CH4}$) are powerful geochemical indicators for revealing the microbial pathways of biogenic CH_4 (Whiticar and Faber, 1986; Whiticar, 1999; Pohlman et al., 2009; Kim et al., 2012). In general, the ε_c value of CO_2 reduction in marine sediments ranges from 49‰ to over 100‰, mostly approximately 65‰–75‰. Oppositely, it is notably lower, typically ranging between 40‰ and 55‰, resulting from the fermentation of methylated substrates in freshwater environments (Whiticar et al., 1986; Whiticar, 1999; Whiticar and Elvert, 2001; Pohlman et al., 2009). We estimated the ε_c values of the HS, VG, and BG gases since the CH_4 at the ARAON Mounds and background sites is influenced by a biogenic source.

The estimated ε_c values of the HS gases at Site ARA09C-St 08 range from 61‰ to 65‰, which are consistent with methanogenesis driven predominantly by microbial CO_2 reduction. On the other hand, the ε_c values of the HS gases at Sites ARA07-St 13, ARA07-St 14, ARA09C-St 04, ARA09C-St 06, ARA09C-St 07, and ARA09C-St 12 vary from 17‰ to 50‰, which are remarkably lower than those from CO_2 reduction (Fig. 7). In addition, these values decrease below the SMT (<25‰) compared to those above the SMT (>30‰) at Sites ARA09C-St 04, ARA09C-St 07, and ARA09C-St 12 (Supplementary Table 2). Hence, the estimated ε_c value suggests that the CH_4 at the ARAON Mounds originates from either methyl fermentation in freshwater or is affected by AOM. However, the dissolved SO_4^{2-} profile in the pore water and the gas isotopic data ($\delta^{13}C_{CH4}$, $\delta^{13}C_{C2H6}$, and δD_{CH4}) deviate from this finding. All sites at the ARAON Mounds exhibit the SMT; thus, the effect of AOM is not exerted along the entire coring depth but to limited intervals near the SMT. In addition, CH_4 is generated by methanogenesis via CO_2 reduction over methyl fermentation above the SMT, and it predominantly originates from a thermogenic source below the SMT at the ARAON Mounds. Kim et al. (2012) reported abnormally low ε_c values at chimney sites in the Ulleung Basin with a biogenic CH_4 source, which is accounted for by the two-phase transportation model. Since the solubility of CH_4 is very low relative to that of CO_2 at the same pressures and temperatures (Duan et al., 2006; Sun and Duan, 2007) and CH_4 does not exhibit any significant carbon fractionation at the gas/water interface, there is a decoupling of CH_4 from the CO_2 pool during gas migration, resulting in abnormally low ε_c values. Similarly, as shown in Fig. 7, the enriched $^{13}CH_4$ generated from a thermogenic source in deep-seated sediments is transported toward the seafloor, which is higher than that of the Ulleung Basin (−75‰ to −65‰), and the CH_4 produced by CO_2 reduction above/near the SMT is mixed with the thermogenic CH_4 near the SMT at the nonhydrate-bearing sites (ARA09C-St 04, ARA09C-St 07, and ARA09C-St 12) of the ARAON Mounds. In contrast, enriched $^{12}CO_2$ is generated by microbial activity within the retrieved core, which has not shown a significant difference between the sections above and below the SMT, and the measured $\delta^{13}C_{CO2}$ value at those sites has a similar range as that in the Ulleung Basin (−51‰ to −15‰; Fig. 7). Consequently, the ε_c values below the SMT at those sites are much lower than those below the SMT in the Ulleung Basin (30‰–46‰) and fall in the AOM region because the deep-sourced CH_4 is thermogenic at the ARAON Mounds with enriched $^{13}CH_4$ values that are at least 10‰ higher than those in the Ulleung Basin. On the other hand, the ε_c values in the HS samples from Sites ARA09C-St 06 and ARA09C-St 16, where gas hydrates were encountered, are clearly distinct from those in the HS samples from the nonhydrate-bearing sites at the ARAON Mounds (Fig. 7). Additionally, the ε_c values usually show an enriched trend with the depth because $\delta^{13}C_{CO2}$ increases, while $\delta^{13}C_{CH4}$ remains relatively constant with the depth at the hydrate-bearing sites of the ARAON Mounds (Fig. 7; Supplementary Table 2). Most likely, the influence of the biogenic CO_2 with enriched ^{12}C transport at the hydrate-bearing sites is smaller than that at the nonhydrate-bearing sites of the ARAON Mounds due to the high gas migration flux from the deep-seated sediments. Hence, the ε_c values at the hydrate-bearing sites of the ARAON Mounds in the study area are deviated from both methyl fermentation and methane oxidation and are clearly distinct from those at the nonhydrate-bearing sites (Fig. 7). In combination with the ε_c values at the ARAON Mounds and in the Ulleung Basin, we postulate that the anomalously low ε_c values definitely indicate upward gas migration irrespective of the gas source, and the nonhydrate- and

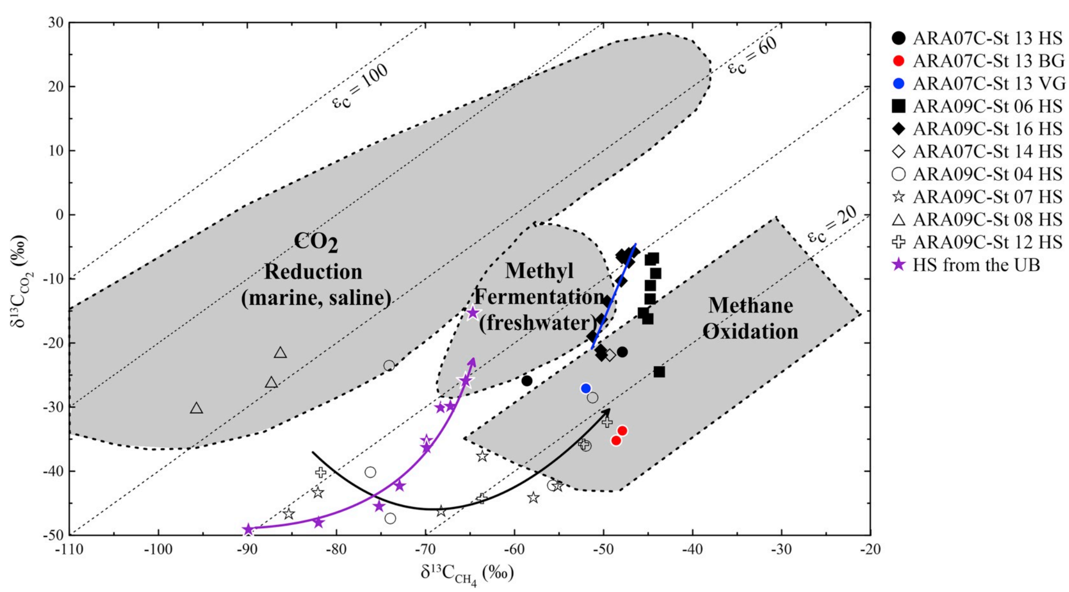

Fig. 7. Estimated ε_c ($\delta^{13}C_{CO2}$ - $\delta^{13}C_{CH4}$) with isotopic fractionation lines (adapted Kim et al., 2012). HS gases from Site ARA09C-St 08 (background site) are fall in the CO_2 reduction region, while HS gases from the nonhydrate-bearing sites (ARA09C-St 04 and ARA09C-St 07) deviate significantly from the CO_2 reduction region and plot along the black line, which is significantly different trend compared to the HS samples (violet stars) from the chimney sites in the Ulleung Basin (UB) followed the violet line (data from Kim et al., 2012). HS gases from the hydrate-bearing sites (ARA09C-St 06 and ARA09C-St 16) remarkably discriminate with that from the nonhydrate-bearing sites. The estimated ε_c of HS gases from hydrate-bearing sites shows the increasing trend with sampling depth (e.g., blue line from Site ARA09C-St 16). HS shown in black open symbols at the nonhydrate-bearing sites whereas HS in black closed symbols, VG in blue closed symbols, and BG in red closed symbols at the hydrate-bearing sites.

hydrate-bearing sites in both areas are distinctly different. Thus, these values can be useful geochemical indicators to infer gas hydrate existence and methane migration generated by both thermogenic and biogenic sources.

6. Conclusions

1. The isotopic signatures of the void and hydrate-bound gases at the ARAON Mounds indicate that methane and ethane originated from thermogenic sources have migrated from deep-seated sediments (>1 km) toward the seafloor through faults/fractures.
2. The isotopic signatures of HS gases from the nonhydrate-bearing sites suggest three CH_4 sources increase with depth (a biogenic source above the SMT, a mixed source above/near the SMT, and a thermogenic source below the SMT), while CH_4 predominately originates from a thermogenic source at the hydrate-bearing sites. Hence, the CH_4 source promptly changes vertically and horizontally at the ARAON Mounds depending on the occurrence of gas hydrate seafloor. These results are associated with the amount of upwardly deep-sourced thermogenic gas because the migrated gas can supply enough CH_4 to form gas hydrate in the shallow sediments at the hydrate-bearing sites. On the other hand, the biogenic CH_4 and CO_2 produced above/near the SMT affect the isotopic signatures at the nonhydrate-bearing sites.
3. The HS, void, and hydrate-bound gases have high C_1/C_{2+} ratios (>300) at the ARAON Mounds, indicating that they are altered by postgenetic processes during the migration of deep-sourced thermogenic gases rather than by thermal cracking of C_{2+}.
4. The estimated ε_c values at the ARAON Mounds are anomalously low, which is also significantly lower than those at chimney sites formed by biogenic hydrocarbon sources. Additionally, the estimated ε_c value is clearly different between the hydrate- and nonhydrate-bearing sites at these mounds because of the gas flux difference between these sites. Consequently, we postulate that the ε_c value can be useful as a geochemical proxy to identify high gas fluxes and the occurrence of gas hydrates in shallow sediments irrespective of the gas source.

Declaration of competing interest

The authors declare that they have no known competing financial interests or personal relationships that could have appeared to influence the work reported in this paper.

CRediT authorship contribution statement

Ji-Hoon Kim: Conceptualization, Visualization, Writing - original draft. **Akihiro Hachikubo:** Formal analysis, Data curation, Writing - review & editing. **Masato Kida:** Investigation, Writing - review & editing. **Hirotsugu Minami:** Investigation, Writing - review & editing. **Dong-Hun Lee:** Investigation, Writing - review & editing. **Young Keun Jin:** Investigation, Writing - review & editing. **Jong-Sik Ryu:** Investigation, Writing - review & editing. **Yung Mi Lee:** Investigation, Writing - review & editing. **Jin Hur:** Investigation, Writing - review & editing. **Myong-Ho Park:** Investigation, Writing - review & editing. **Young-Gyun Kim:** Investigation, Writing - review & editing. **Moo-Hee Kang:** Writing - review & editing, Data curation. **Sanghee Park:** Writing - review & editing, Data curation. **Meilian Chen:** Writing - review & editing, Data curation. **Seung-Goo Kang:** Writing - review & editing, Data curation. **Sookwan Kim:** Formal analysis.

Acknowledgements

We would like to thank the captain and crew of the *IBRV* ARAON for their help at sea. This study was made possible with the funding support from the Korean Ministry of Oceans and Fisheries (NP2018-022 and Project No. 20160247) and from Korean Ministry of Science and ICT (GP2016-027 and GP2017-018). In addition, we acknowledge support from Korean Ministry of Trade, Industry and Energy (Project No. 20162010201980) to M.-H. Park; and from Basic Science Research Program through the National Research Foundation of Korea (NRF) funded by Korean Ministry of Education (No. 2019R1A6A1A03033167) to Y.-G. Kim.

Appendix A. Supplementary data

Supplementary data to this article can be found online at https://doi.org/10.1016/j.jngse.2020.103223.

References

Arthur, M.A., Dean, W.D., Laarkamp, K., 1998. Organic carbon accumulation and preservation in surface sediments on the Peru margin. Chem. Geol. 152, 273–286.
Bernard, B.B., Brooks, J.M., Sackett, W.M., 1976. Natural gas seepage in the Gulf of Mexico. Earth Planet Sci. Lett. 31, 48–54.
Bernard, B.B., Brooks, J.M., Sackett, W.M., 1978. Light hydrocarbons in recent Texas continental shelf and slope sediments. J. Geophys. Res. 83, 4053–4061.
Borowski, W.S., Paull, C.K., Ussler III., W., 1996. Marine pore-water sulfate profiles indicate in situ methane flux from underlying gas hydrate. Geology 24, 655–658.
Brigham-Grette, J., Hopkins, D.M., Ivanov, V.F., Basilyan, A.E., Benson, S.L., Heiser, P.A., Pushkar, V.S., 2001. Last interglacial (isotope stage 5) glacial and sea-level history of coastal Chukotka Peninsula and St. Lawrence Island, Western Beringia. Quat. Sci. Rev. 20, 419–436.
Coffin, R.B., Smith, J.P., Plummer, R.E., Yoza, B., Larsen, R.K., Millholland, L., Montgomery, M.T., 2013. Spatial variation in shallow sediment methane sources and cycling on the Alaskan Beaufort Sea Shelf/Slope. Mar. Petrol. Geol. 45, 186–197. https://doi.org/10.1016/j.marpetgeo.2013.05.002.
Dlugokencky, E.J., Bruhwiler, L., White, J.W.C., Emmons, L.K., Novelli, P.C., Montzka, S. A., Masarie, K.A., Lang, P.M., Crotwell, A.M., Miller, J.B., Gatti, L.V., 2009. Observational constraints on recent increases in the atmospheric CH_4 burden. Geophys. Res. Lett. 36, L18803. https://doi.org/10.1029/.2009GL039780.
Dove, D., Polyak, L., Coakley, B., 2014. Widespread, multi-source glacial erosion on the Chukchi margin, Arctic Ocean. Quat. Sci. Rev. 92, 112–122. https://doi.org/10.1016/j.quascirev.2013.07.016.
Duan, Z., Sun, R., Zhu I.M., C., 2006. An improved model for the calculation of CO_2 solubility in aqueous solutions containing Na^+, K^+, Ca^{2+}, Mg^{2+}, Cl^-, and SO_4^{2-}. Mar. Chem. 98, 131–139. https://doi.org/10.1016/j.marchem.2005.09.001.
Fischer, D., Mogollon, J.M., Strasser, M., Pape, T., Bohrmann, G., Fekete, N., Spiess, V., Kasten, S., 2013. Sub-duction zone earthquake as potential trigger of submarine hydrocarbon seepage. Nat. Geosci. 6, 647–651. https://doi.org/10.1038/ngeo1886.
Grantz, A., Clark, D.L., Phillips, R.L., Srivastava, S.P., Blome, C.D., Gray, L.B., Haga, H., Mamet, B.L., McIntyre, D.J., McNeil, D.H., Mickey, M.B., Mullen, M.W., Murchey, B. I., Ross, C.A., Stevens, C.H., Silberling, N.J., Wall, J.H., Willard, D.A., 1998. Phanerozoic stratigraphy of Northwind Ridge, magnetic anomalies in the Canada basin, and the geometry and timing of rifting in the Amerasia basin, Arctic Ocean, 110. Geological Society of America Bulletin, pp. 801–820.
Grebmeier, J.M., McRoy, C.P., Feder, H.M., 1988. Pelagic-benthic coupling on the shelf of the northern Bering and Chukchi Seas. I. Food supply source and benthic biomass. Mar. Ecol. Prog. Ser. 48, 57–67.
Gualtieri, L., Vartanyan, S.L., Brigham-Grette, J., Anderson, P.M., 2005. Evidence for an ice-free Wrangel Island, northeast Siberia during the last glacial maximum. Boreas 34, 264–273. https://doi.org/10.1111/j.1502-3885.2005.tb01100.x.
Hachikubo, A., Khlystov, O., Krylov, A., Sakagami, H., Minami, H., Nunokawa, Y., Yamashita, S., Takahashi, N., Shoji, H., Nishio, S., Kida, M., Ebinuma, T., Kalmychkov, G., Poort, J., 2010. Molecular and isotopic characteristics of gas hydrate-bound hydrocarbons in southern and central Lake Baikal. Geo Mar. Lett. 30, 321–329. https://doi.org/10.1007/s00367-010-0203-1.
Hegewald, A., Jokat, W., 2013. Tectonic and sedimentary structures in the northern Chukchi region, Arctic Ocean. J. Geophys. Res.: Solid Earth 118, 3285–3296. https://doi.org/10.1002/jgrb.50282.
Hensen, C., Zabel, M., Pfeifer, K., Schwenk, T., Kasten, S., Riedinger, N., Schulz, H.D., Boetius, A., 2003. Control of sulfate pore-water profiles by sedimentary events and the significance of anaerobic oxidation of methane for the burial of sulfur in marine sediments. Geochim. Cosmochim. Acta 67, 2631–2647.
Hong, W.L., Torres, M.E., Carroll, J., Cremiere, A., Panieri, G., Yao, H., Serov, P., 2017. Seepage from an Arctic shallow marine gas hydrate reservoir is insensitive to momentary ocean warming. Nat. Commun. https://doi.org/10.1038/ncomms15745.
Hong, W.L., Torres, M.E., Portnov, A., Waage, M., Haley, B., Lepland, A., 2018. Variations in gas and water pulses at an Arctic seep: fluid sources and methane transport. Geophys. Res. Lett. 45, 4153–4162. https://doi.org/10.1029/2018GL077309.
Hunt Jr., G.L., Blanchard, A.L., Boveng, P., Dalpadado, P., Drinkwater, K.F., Eisner, L., Hopcroft, R.R., Kovacs, K.M., Norcross, L., Renaud, P., Reigstad, M., Renner, M., Skjolda, H.R., Whitehouse, A., Woodgate, R.A., 2013. The Barents and Chukchi Seas: comparison of two Arctic shelf ecosystems. J. Mar. Syst. 109–110, 43–68. https://doi.org/10.1016/j.jmarsys.2012.08.003.

Ilhan, I., Coakley, B.J., 2018. Meso-cenozoic evolution of the southwestern Chukchi Borderland, Arctic Ocean. Mar. Petrol. Geol. 95, 100–109. https://doi.org/10.1016/j.marpetgeo.2018.04.014.

IPCC, 2013. Climate Change 2013- the Physical Science Basis-Contribution of Working Group I to the Fifth Assessment Report of the Intergovernmental Panel on Climate Change. Cambridge University Press, Cambridge.

Jakobsson, M., 2002. Hypsometry and volume of the Arctic Ocean and its constituent seas. Geochem. Geophys. Geosyst. 3, 1028. https://doi.org/10.1029/2001GC000302.

Jakobsson, M.J., Gardner, V., Vogt, P., Mayer, L.A., Armstrong, A., Backman, J., Brennan, R., Calder, B., Hall, J.K., Kraft, B., 2005. Multibeam bathymetric and sediment profiler evidence for ice grounding on the Chukchi Borderland, Arctic Ocean. Quat. Res. 63, 150–160. https://doi.org/10.1016/j.yqres.2004.12.004.

Jakobsson, M., Nilsson, J., O'Regan, M., Backman, J., Löwemark, L., Dowdeswell, J.A., Polyak, L., Colleoni, F., Anderson, L.G., Bjork, G., Darby, D., Eriksson, B., Hanslik, D., Hell, B., Marcussen, C., Sellen, E., Wallin, A., 2010. An Arctic Ocean ice shelf during MIS 6 constrained by new geophysical and geological data. Quat. Sci. Rev. 29, 3505–3517. https://doi.org/10.1016/j.quascirev.2010.03.015.

James, A.T., Burns, B.J., 1984. Microbial alteration of subsurface natural gas accumulations. AAPG (Am. Assoc. Pet. Geol.) Bull. 68, 957–960.

Jin, Y.K., Shipboard Scientific Party, 2017. ARA07C Cruise Report: 2016 Korea-Russia-Germany East Siberian Sea Research Program. Korea Polar Research Institute, Korea Polar Research Institute, p. 103.

Jin, Y.K., Shipboard Scientific Party, 2019. ARA09C Cruise Report: 2018 Korea-Russia-Japan East Siberian/Chukchi Sea Research Program. Korea Polar Research Institute, Korea Polar Research Institute, p. 205.

Kasten, S., Nothen, K., Hensen, C., Spiess, V., Blumenberg, M., Schneider, R.R., 2012. Gas hydrate decomposition recorded by authigenic barite at pockmark sites of the northern Congo Fan. Geo Mar. Lett. 32, 515–524. https://doi.org/10.1007/s00367-012-0288-9.

Kerr, R., 2010. 'Arctic armageddon' needs more science, less hype. Science 329, 620–621. https://doi.org/10.1126/science.329.5992.620.

Kim, J.-H., Park, M.-H., Chun, J.-H., Lee, J.Y., 2011. Molecular and isotopic signatures in sediments and gas hydrate of the central/southwestern Ulleung Basin: high alkalinity escape fuelled by biogenically sourced methane. Geo Mar. Lett. 31, 37–49. https://doi.org/10.1007/s00367-010-0214-y.

Kim, J.-H., Torres, M.E., Choi, J., Bahk, J.-J., Park, M.-H., Hong, W.-L., 2012. Inferences on gas transport based on molecular and isotopic signatures of gases at acoustic chimneys and background sites in the Ulleung Basin. Org. Geochem. 43, 26–38. https://doi.org/10.1016/j.orggeochem.2011.11.004.

Kim, J.-H., Torres, M.E., Lee, J.Y., Hong, W.-L., Holland, M., Park, M.-H., Choi, J., Kim, G.-Y., 2013. Depressurization experiment of pressure cores from the central Ulleung Basin, East Sea: insights into gas chemistry. Org. Geochem. 62, 86–95. https://doi.org/10.1016/j.orggeochem.2013.07.010.

Lafargue, E., Espitalié, J., Marquis, F., Pillot, D., 1998. Rock-Eval 6 applications in hydrocarbon exploration, production and soil contamination studies. Rev. Inst. Fr. Petrol 53, 421–437.

Mau, S., Römer, M., Torres, M.E., Bussmann, I., Pape, T., Damm, E., Geprägs, P., Wintersteller, P., Hsu, C.-W., Loher, M., Bohrmann, G., 2017. Widespread methane seepage along the continental margin off Svalbard-from Bjørnøya to Kongsfjorden. Sci. Rep. 7, 42997. https://doi.org/10.1038/srep42997.

McGuire, A.D., Anderson, L.G., Christensen, T.R., Dallimore, S., Guo, L., Hayes, D.J., Heimann, M., Lorenson, T.D., Macdonald, R.W., Roulet, N., 2009. Sensitivity of the carbon cycle in the Arctic to climate change. Ecol. Monogr. 79, 523–555. https://doi.org/10.1890/08-2025.1.

Milkov, A.V., 2005. Molecular and stable isotope compositions of natural gas hydrates: a revised global dataset and basic interpretations in the context of geological settings. Org. Geochem. 36, 681–702. https://doi.org/10.1016/j.orggeochem.2005.01.010.

Milkov, A.V., Etiope, G., 2018. Revised genetic diagrams for natural gases based on a global dataset of >20,000 samples. Org. Geochem. 125, 109–120. https://doi.org/10.1016/j.orggeochem.2018.09.002.

Milkov, A.V., Claypool, G.E., Lee, Y.-J., Sassen, R., 2005. Gas hydrate systems at Hydrate Ridge offshore Oregon inferred from molecular and isotopic properties of hydrate-bound and void gases. Geochim. Cosmochim. Acta 69, 1007–1026. https://doi.org/10.1016/j.gca.2004.08.021.

Nali, M., Caccialanza, G., Ghiselli, C., Chiaramonte, M.A., 2000. T_{max} of asphaltenes: A parameter for oil maturity assessment. Org. Geochem. 31, 1325–1332.

Niessen, F., Hong, J.K., Hegewald, A., Matthiessen, J., Stein, R., Kim, H., Kim, S., Jensen, L., Jokat, W., Nam, S.-I., Kang, S.-H., 2013. Repeated Pleistocene glaciation of the East Siberian continental margin. Nat. Geosci. 6, 842–846. https://doi.org/10.1038/ngeo1904.

Nothen, K., Kasten, S., 2011. Reconstructing changes in seep activity by means of pore water and solid phase Sr/Ca and Mg/Ca ratios in pockmark sediments of the Northern Congo Fan. Mar. Geol. 287, 1–13. https://doi.org/10.1016/j.margeo.2011.06.008.

Pape, T., Bahr, A., Rethemeyer, J., Kessler, J.D., Sahling, H., Hinrichs, K.-U., Klapp, S.A., Reeburgh, W.S., Bohrmann, G., 2010. Molecular and isotopic partitioning of low molecular-weight hydrocarbons during migration and gas hydrate precipitation in deposits of a high-flux seepage site. Chem. Geol. 269, 350–363. https://doi.org/10.1016/j.chemgeo.2009.10.009.

Pape, T., Feseker, T., Kasten, S., Fischer, D., Bohrmann, G., 2011. Distribution and abundance of gas hydrates in near- surface deposits of the Håkon Mosby Mud Volcano, SW Barents Sea. Geochem. Geophys. Geosyst. 12, Q09009. https://doi.org/10.1029/2011GC00357.

Paull, C.K., Normark, W.R., Ussler III, W., Caress, D.W., Keaten, R., 2008. Association among active seafloor deformation, mound formation, and gas hydrate growth and accumulation within the seafloor of the Santa Monica Basin, offshore California. Mar. Geol. 258–275. https://doi.org/10.1016/j.margeo.2008.01.011.

Paull, C.K., Dallimore, S.R., Caress, D.W., Gwiazda, R., Melling, H., Riedel, M., Jin, Y.K., Hong, J.K., Kim, Y.-G., Graves, D., Sherman, A., Lundsten, E., Anderson, K., Lundsten, L., Villinger, H., Kopf, A., Johnson, S.B., Hughes Clarke, J., Blasco, S., Conway, K., Neelands, P., Thomas, H., Cote, M., 2015. Active mud volcanoes on the continental slope of the Canadian Beaufort Sea. Geochem. Geophys. Geosyst. 16, 3160–3181. https://doi.org/10.1002/2015GC005928.

Pernaton, E., Prinzhofer, A., Schneider, F., 1996. Reconsideration of methane signature as a criterion for the genesis of natural gas: influence of migration on isotopic signature. Rev. Inst. Fr. Petrol 51, 635–651.

Pimmel, A., Claypool, G., 2001. Introduction to Shipboard Organic Geochemistry on the JOIDES Resolution, vol. 30. Ocean Drilling Program Technical Note, College Station, TX.

Plaza-Faverola, A., Vadakkepuliyambatta, S., Hong, W.-L., Mienert, J., Bünz, S., Chand, S., Greinert, J., 2017. Bottom-simulating reflector dynamics at Arctic thermogenic gas provinces: an example from Vestnesa Ridge, offshore west Svalbard. J. Geophys. Res.: Solid Earth 122, 4089–4105. https://doi.org/10.1002/2016JB013761.

Pohlman, J.W., Kaneko, M., Heuer, V.B., Coffin, R.B., Whiticar, M., 2009. Methane sources and production in the northern Cascadia margin gas hydrate system. Earth Planet Sci. Lett. 287, 504–512. https://doi.org/10.1016/j.epsl.2009.08.037.

Polyak, L., Edwards, M.H., Coakley, B.J., Jakobsson, M., 2001. Ice shelves in the Pleistocene Arctic Ocean inferred from glaciogenic deep-sea bedforms. Nature 410, 453–459.

Polyak, L., Darby, V.D.A., Bischoff, J.F., Jakobsson, M., 2007. Stratigraphic constraints on late Pleistocene glacial erosion and deglaciation of the Chukchi margin, Arctic Ocean. Quat. Res. 67, 234–245. https://doi.org/10.1016/j.yqres.2006.08.001.

Price, L.C., Schoell, M., 1995. Constraints on the origins of hydrocarbon gas from compositions of gases at their site of origin. Nature 378, 368–371.

Prinzhofer, A., Huc, A.Y., 1995. Genetic and post-genetic molecular and isotopic fractionations in natural gases. Chem. Geol. 126, 281–290.

Prinzhofer, A., Pernaton, E., 1997. Isotopically light methane in natural gas: bacterial imprint or diffusive fractionation? Chem. Geol. 142, 193–200.

Sajgó, C., 2000. Assessment of generation temperatures of crude oils. Org. Geochem. 31, 1301–1323.

Sassen, R., Joye, S., Sweet, S.T., DeFreitas, D.A., Milkov, A.V., MacDonald, I.R., 1999. Thermogenic gas hydrates and hydrocarbon gases in complex chemosynthetic communities, Gulf of Mexico continental slope. Org. Geochem. 30, 485–497.

Schoell, M., 1984a. Isotope studies in petroleum research. In: Brooks, J., Welte, D. (Eds.), Advances in Petroleum Geochemistry, vol. 1, pp. 215–245.

Schoell, M., 1984b. Recent advances in petroleum isotope geochemistry. Org. Geochem. 6, 645–663.

Schoell, M., 1988. Multiple origins of methane in the earth. Chem. Geol. 71, 1–10.

Shakhova, N., Semiletov, I., Panteleev, G., 2005. The distribution of methane on the East Siberian Arc tic shelves: implications for the marine methane cycle. Geophys. Res. Lett. 32, L09601. https://doi.org/10.1029/.2005GL02275.

Shakhova, N., Semiletov, I., Salyuk, A., Yusupov, V., Kosmach, D., Gustafsson, O., 2010. Extensive methane venting to the atmosphere from sediments of the East Siberian Arctic shelf. Science 327, 1246–1250. https://doi.org/10.1126/science.1182221.

Stahl, W.J., Carey, B.D., 1975. Source-rock identification by isotope analyses of natural gases from fields in the Val Verde and Delaware basins, west Texas. Chem. Geol. 16, 257–267.

Stolper, D.A., Lawson, M., Davis, C.L., Ferreira, A.A., Santos Neto, E.V., Ellis, G.S., Lewan, M.D., Martini, A.M., Tang, Y., Schoell, M., Sessions, A.L., Eiler, J.M., 2014. Formation temperatures of thermogenic and biogenic methane. Science 344, 1500–1503. https://doi.org/10.1126/science.1254509.

Suess, E., Bohrmann, G., Greinert, J., Lausch, E., 1999. Flammable ice. Sci. Am. 281, 76–83.

Sun, R., Duan, Z., 2007. An accurate model to predict the thermodynamic stability of methane hydrate and methane solubility in marine environments. Chem. Geol. 244, 248–262. https://doi.org/10.1016/j.chemgeo.2007.06.021.

Tissot, B.P., Welte, D.H., 1984. Petroleum Formation and Occurrence, second ed. Springer-Verlag, Berlin, p. 699.

Ussler III., W., Paull, C.K., 2008. Rates of anaerobic oxidation of methane and authigenic carbonate mineralization in methane-rich deep-sea sediments inferred from models and geochemical profiles. Earth Planet Sci. Lett. 266, 271–287. https://doi.org/10.1016/j.epsl.2007.10.056.

Waage, M., Portnov, A., Serov, P., Bünz, S., Waghorn, K.A., Vadakkepuliyambatta, S., Mienert, J., Andreassen, K., 2019. Geological controls on fluid flow and gas hydrate pingo development on the Barents Sea margin. Geochem. Geophys. Geosyst. 20, 630–650. https://doi.org/10.1029/2018GC007930.

Weingartner, T., Aagaard, K., Woodgate, R., Danielson, S., Sasaki, Y., Cavalieri, D., 2005. Circulation on the north central Chukchi Sea shelf. Deep Sea Res. Part II Top. Stud. Oceanogr. 52, 3150–3174. https://doi.org/10.1016/j.dsr2.2005.10.015.

Westbrook, G.K., Thatcher, K.E., Rohling, E.J., Piotrowski, A.M., Pälike, H., Osborne, A. H., Nisbet, E.G., Minshull, T.A., Lanoisellé, M., James, R.H., Hühnerbach, V., Green, D., Fisher, R.E., Crocker, A.J., Chabert, A., Bolton, C., Beszczynska-Möller, A., Berndt, C., Aquilina, A., 2009. Escape of methane gas from the seabed along the West Spitsbergen continental margin. Geophys. Res. Lett. 36, L15608. https://doi.org/10.1029/2009GL039191.

Whiticar, M.J., 1999. Carbon and hydrogen isotope systematics of bacterial formation and oxidation of methane. Chem. Geol. 161, 291–314.

Whiticar, M.J., Faber, E., 1986. Methane oxidation in sediment and water column environments- isotope evidence. Org. Geochem. 10, 759–768.

Whiticar, M.J., Elvert, M.E., 2001. Organic geochemistry of saanich inlet, BC, during the Holocene as revealed by ocean drilling program leg 169S. Mar. Geol. 174, 249–271.

Whiticar, M.J., Faber, E., Schoell, M., 1986. Biogenic methane formation in marine and freshwater environments: CO_2 reduction vs. acetate fermentation-isotope evidence. Geochim. Cosmochim. Acta 50, 693–709.

Wilhelms, A., Larter, S.R., Head, I., Farrimond, P., di-Primio, R., Zwach, C., 2001. Biodegradation of oil in uplifted basins prevented by deep-burial sterilization. Nature 411, 1034–1037.

Wilson, R.M., Macelloni, L., Simonetti, A., Lapham, L., Lutken, C., Sleeper, K., D'Emidio, M., Pizzi, M., Knapp, J., Chanton, J., 2014. Subsurface methane sources and migration pathways within a gas hydrate mound system, Gulf of Mexico. Geochem. Geophys. Geosyst. 15, 89–107. https://doi.org/10.1002/2013GC004888.

Woodgate, R.A., Aagaard, K., 2005. Revising the bering strait freshwater flux into the Arctic Ocean. Geophys. Res. Lett. 32, L02602. https://doi.org/10.1029/2004GL021747.

Zabel, M., Schulz, H.D., 2001. Importance of submarine landslides for non-steady state conditions in pore water systems-lower Zaire (Congo) deep-sea fan. Mar. Geol. 176, 87–99.